Soft Matter

Accepted Manuscript

ROYAL SOCIETY OF CHEMISTRY

www.rsc.org/softmatter

Soft Matter

RSCPublishing

ARTICLE

Correlation between Geometrical Shape and Growth Behaviour of Surfactant Micelles Investigated with Small-Angle Neutron Scattering

Cite this: DOI: 10.1039/xoxxoooooox

Received ooth January 2014,
Accepted ooth January 2014

DOI: 10.1039/xoxxoooooox

www.rsc.org/

L.M. Bergström*[a] and I. Grillo[b],

The correlation between growth behaviour and geometrical shape for CTAB-rich mixed micelles formed by the cationic surfactant hexadecyl trimtheyl ammonium bromide (CTAB) and the anionic surfactant sodium octyl sulphate (SOS) has been investigated with small-angle neutron scattering (SANS). Rather small tablet-shaped micelles formed by CTAB are found to grow only weakly in size with increasing surfactant concentration. The extent of growth becomes increasingly stronger as the fraction of SOS is increased. At higher fractions of SOS, a rather weak growth at low surfactant concentrations is followed by a sharp increase in aggregation numbers beyond a certain surfactant concentration. Such an abrupt transition from weakly to strongly growing micelles has been observed in the past for several micellar systems and is usually referred to as *the second critical micelle concentration*. The growth behaviour has been rationalized from a theoretical point of view by means of employing the recently developed *general micelle model*. The theory excellently predicts micellar growth behaviours as well as the observed correlation between geometrical shape and micellar growth. In accordance, both width and length are found to slightly increase for weakly growing tablet-shaped micelles. On the other hand, strongly growing micelles that are observed above the second cmc display a completely different behaviour, according to which the length increases considerably while the width of the micelles decreases. Most interestingly, by means of optimizing the agreement between the general micelle model and experimentally determined aggregation numbers, we are able to determine the three bending elasticity constants spontaneous curvature, bending rigidity and saddle-splay constant.

1. Introduction

It is well-known that surfactant micelles grow in size with increasing surfactant concentration. It was demonstrated by Tanford[1] that, according to simple geometrical constraints, micelles can only be strictly spherically shaped below a certain aggregation number corresponding to a radius equal to the length of a surfactant molecule. Thus, a micelle must assume some kind of non-spherical shape as it grows beyond a certain aggregation number. A typical feature displayed by several micellar systems shows that micelles grow weakly at low surfactant concentration and begin to grow more strongly above a certain concentration usually denoted the second critical micelle concentration (second cmc).[2-7] This transition from weakly to strongly growing micelles has often been interpreted as due to a transition from spherical to rodlike micelles, a so called sphere-to-rod transition. However, the aggregation numbers of micelles at the second cmc have usually been found to largely exceed values consistent with a spherical micellar shape according to the geometrical analysis of Tanford.

The geometrical shape of micelles may be determined with small-angle neutron scattering (SANS). It is well known that the small-angle scattering data of rather small and weakly growing micelles formed by, for instance, sodium dodecyl sulphate (SDS) and hexadecyl trimethylammonium bromide (CTAB) is not at all compatible with the assumption of a model for monodisperse and strictly spherical micelles.[8-10] The agreement between experimental data and model may be significantly improved by assuming spherical micelles to be highly polydisperse, *i.e.* about 0.2-0.25 with respect to radius R corresponding to 70-75 % with respect to aggregation number N (see the Electronic Supplementary Information (ESI) for the derivation of a relation between $\sigma_R/\langle R\rangle$ and $\sigma_N/\langle N\rangle$).[8,10] However, such a high polydispersity contradicts the observation of a weak growth behaviour of these micelles as may be deduced from the following important relation

$$\left(\frac{\sigma_N}{\langle N\rangle}\right) = \sqrt{\frac{d\ln\langle N\rangle}{d\ln\phi_t}} \quad (1)$$

derived by Hall and Pethica[11] and shown in detail in the ESI.

According to eqn (1), $\sigma_N/\langle N\rangle$ = 0.7-0.75 corresponds to a much stronger growth behaviour, $d\ln\langle N\rangle/d\ln\phi_t \approx$ 0.5-0.55, than consistent with experimental observations, *i.e.* 0.15 for SDS[12,13] and about 0.125 for CTAB (see further below).

It is well known that long rodlike or wormlike micelles may grow more strongly than anticipated by spherocylindrical micelles that grow exclusively in the length direction.[3,14-16] Moreover, it has previously been demonstrated from small-angle neutron scattering (SANS) measurements that ordinary surfactant micelles are not usually shaped as spheres or spherocylinders but are, in fact, shaped as triaxial tablets that may grow both with respect to width and length.[9,10,17-21] Hence, in order to rationalize as well as generate a detailed understanding of the growth behaviour of surfactant micelles it is of decisive importance to correlate the growth behaviour of micelles with their geometrical shape.

In the present paper we investigate micelles formed in CTAB-rich mixtures of sodium octyl sulphate (SOS) and CTAB, the growth behaviours of which are found to be strongly dependent on surfactant composition, with SANS in order to correlate the growth behaviour with the detailed geometrical shape of the micelles. Our experimental results are compared and rationalized with predictions deduced from a recently derived theoretical model - the general micelle model[22] - based on thermodynamics of self-assembly combined with bending elasticity theory. Below we demonstrate that, as a result of our combined experimental and theoretical study, we are able to rationalize the growth behaviours of ordinary surfactant micelles in terms of the three bending elasticity constants spontaneous curvature (H_0), bending rigidity (k_c) and saddle-splay constant ($\overline{k}_c$).

2. Experimental

2.1 Sample preparation

Stock solutions containing hexadecyltrimethylammonium bromide (CTAB) and sodium octyl sulphate (SOS) with [SOS] + [CTAB] = 40 mM and surfactant compositions equal to $y \equiv$ [SOS]/([SOS] + [CTAB]) = 0, 0.05, 0.10, 0.20 and 0.25 were prepared in deuterium oxide (D_2O) by simply mixing the two surfactants with D_2O. The final samples were obtained by means of diluting the stock solutions with pure solvent to obtain a range of total surfactant concentration [SOS] + [CTAB] = 10, 20 and 40 mM. All samples were equilibrated at least 24 hours at 30 °C before measured. The temperature 30 °C was chosen since CTAB precipitates in deuterium oxide below about 29 °C. The Krafft point in CTAB/SOS mixtures decreases with an increasing fraction of SOS. Deuterium oxide was chosen as solvent in order to minimize the incoherent background from hydrogen and obtain a high scattering contrast in the SANS experiments.[23]

2.2 Small-angle neutron scattering

The small-angle neutron scattering (SANS) experiments were carried out at the D33 SANS instrument at Institut Laue-Langevin (ILL), Grenoble, France. The measurements were carried out with the three settings combining sample-to-detector distance d and neutron wavelength λ, *i.e.* [d = 2 m, λ = 4.6 Å], [d = 12.8 m, λ = 4.6 Å] and [d = 12.8 m, λ = 12 Å], giving a range of scattering vectors 0.002-0.29 Å^{-1}. The middle setting was used as the reference setting for the absolute scale. The wavelength resolution was 10 % (full width at half-maximum value).

The samples were kept in quartz cells (Hellma) with path lengths 1 or 2 mm. The raw spectra were corrected for background from the solvent, sample cell and other sources by conventional procedures.[24] The SANS data were set to absolute scale units and normalized by means of dividing with the concentration c_{mic} in [g mL^{-1}] of surfactant (SOS and CTAB) aggregated in micelles, giving the unit [mL g^{-1} cm^{-1}] for the normalized scattering cross-section. The latter may written as

$$\frac{d\sigma_m(q)}{d\Omega} \equiv \frac{1}{c_{mic}}\frac{d\sigma(q)}{d\Omega} = \Delta\rho_m^2 M_w P(q)[1+\beta(q)(S(q)-1)] \quad (2)$$

for weakly interacting dispersed aggregates, where $\Delta\rho_m$ is the difference in scattering length per unit mass solute between particles with a homogeneous core and solvent, M_w is the mass of a single particle and $P(q)$ is the form factor.[25]

The model fits of best quality were obtained by a form factor for either monodisperse triaxial ellipsoids (small micelles) or polydisperse rods with an elliptical cross-section (large and considerably polydisperse micelles). Electrostatic interactions among ion-impenetrable micelles in a rather dilute solution were taken into account using a structure factor $S(q)$ in the rescaled mean spherical approximate (RMSA) as derived by Hansen and Hayter[26], based on the mean spherical approximation (MSA)[27], in combination with a decoupling approximation[28,29]. The introduction of this structure factor introduces three additional fitting parameters related to the relative effective charge of the micelles ($\alpha = z_{eff}/z_{id}$), electrolyte concentration (c_{el}) and concentration of surfactant aggregated in micelles (c_{mic}) (see Table 1 below). The detailed models with form factors are provided in the ESI.

The structure factor is derived for the case of strictly spherical aggregates with charge densities considerably lower than expected for the micelles in our investigated samples. Hence, one cannot expect the values of α, c_{el} and c_{mic} to be highly accurate, although we obtain values of reasonable orders of magnitudes. Nevertheless, we always obtain very good agreement between SANS data and model, which is our main reason for using this structure factor, with a reduced chi-squared always below $\chi^2 = 5$ for the majority of samples and below 10 for all samples except pure CTAB

at 40 mM, despite the very high quality of our SANS data. In this work we are interested in determining the geometry of the micelles, the information of which is mainly provided by scattering data in the high q-range, *i.e.* above about 0.05 Å^{-1}, whereas structure factor effects mainly influence the scattering data in the lowest q-range.[9,25,30-32]

The average excess scattering length density per unit mass of solute (*i.e.* scattering length density divided by density of solute[25]) for SOS in D_2O, $\Delta\rho^m_{SOS} = -4.52\times10^{10}$ cm/g, was calculated using the appropriate molecular volume $\hat{v}_{SOS}$ = 302 Å^3 and molecular weight M_{SOS} = 232.27 g/mol[20,33-35] and CTAB[35], $\Delta\rho^m_{CTAB} = -6.66\times10^{10}$ cm/g, $\hat{v}_{CTAB}$ = 599 Å^3 and M_{CTAB} = 364.45 g/mol. The scattering length density (in units cm/molecule) of mixed micelles has been set equal to $\Delta\rho = x\Delta\rho_{SOS} + (1 - x)\Delta\rho_{CTAB}$, where the mole fraction of SOS in the aggregates x is calculated according to a procedure described in reference 20. This procedure takes into account non-ideal synergistic effects as predicted from the Poisson-Boltzmann mean field theory.[36,37] More details are provided in the ESI.

Throughout the data analysis corrections were made for instrumental smearing. For each instrumental setting the ideal model scattering curves were smeared by the appropriate Gaussian resolution function when the model scattering intensity was compared with the measured absolute scale intensity in least-square model fitting data analysis.[38,39] The parameters in the model were optimized by means of conventional least-squares analysis and the quality of the fits was measured in terms of the reduced chi-squared parameter (χ^2).[25,40]

3. Results and discussion

3.1 SANS measurements of mixed CTAB-rich SOS/CTAB micelles

In recent works we have investigated SOS-rich mixtures of CTAB and SOS.[20,21] Due to the comparatively high critical micelle concentration of SOS (cmc = 133 mM in absence of added salt), we demonstrated that there is a dramatic change in surfactant composition with changes in total surfactant concentration below about the cmc of pure SOS. As a result, we were able to observe micelles growing in size upon simply diluting a sample below about 160 mM, and subsequently a transition to different bilayer aggregates was detected. We demonstrated that the composition in the surfactant aggregates could to be accurately calculated from the Poisson-Boltzmann (PB) mean-field theory[31,37,41] and it was found that the mole fraction of SOS (x) in aggregates formed by two oppositely charged surfactants approaches equimolar composition with decreasing surfactant concentration[20].

In the present paper we investigate micelles formed in CTAB-rich solutions of CTAB and SOS. Since the cmc of CTAB (cmc ≈ 1 mM) is much lower than of SOS, CTAB-rich aggregates behave rather differently from SOS-rich aggregates. In accordance with detailed calculations based on the PB theory, it can be demonstrated that the surfactant composition (x) does not depend on total surfactant concentration (c_t) above about c_t = 10 mM. The results of these calculations are tabulated in the ESI. As a result, we are able to observe mixed CTAB-rich CTAB/SOS micelles growing in size with increasing surfactant concentration in a similar manner as is generally observed in pure surfactant systems.

3.1.1 Results from SANS data analyses. The results from the SANS data analysis of pure CTAB micelles as well as mixed CTAB/SOS micelles are tabulated in Table 1. In pure CTAB solutions as well as in mixtures of CTAB and SOS, with mole fractions of SOS y = 0.05 and 0.10, rather small CTAB-rich micelles are present that were always best fitted with a model for monodisperse tri-axial ellipsoids.

In Fig. 1 SANS data for the sample [CTAB] = 20 mM are shown together with best fittings using models for triaxial general ellipsoidal micelles as well as oblate and prolate spheroidal micelles, respectively. It is seen that the tri-axial ellipsoidal model (χ^2 = 4.3) gives significantly better agreement with data than assuming oblate or prolate spheroids (χ^2 = 6.4 and 7.3, respectively). This difference in fitting quality in favour of triaxial ellipsoidal tablet-shaped micelles holds true for all our investigated samples in which fairly small and monodisperse micelles are present. The micelles are found to grow in size as an increasing amount of oppositely charged surfactant (SOS) is added to the CTAB solutions. As the micelles grow larger, the difference in fitting quality between ellipsoidal and spheroidal models becomes more obvious. For instance, for the sample [y = 0.15, 20 mM] the tri-axial ellipsoidal model still gives excellent agreement with SANS data (χ^2 = 2.3) whereas huge deviations between the oblate (χ^2 = 26.3) and prolate (χ^2 = 60.3) spheroidal models and data are found at scattering vector moduli larger than about q = 0.15 Å^{-1} [*cf.* Fig. 2].

As a consequence of our SANS data analysis, we may thus conclude that the micelles are shaped as triaxial ellipsoidal tablets with three half axes a (related to thickness) < b (related to width) < c (related to length). The three half axes as obtained from our model fitting analysis are plotted in Fig. 3 as functions of the total surfactant concentration c_t ≡ [SOS] + [CTAB] for the two cases pure CTAB micelles (y = 0) and mixed CTAB/SOS micelles with y = 0.10. It is seen that the half axis related to thickness of the micelles (a) is fairly constant with respect to surfactant composition and more or less identical for pure (y = 0) and mixed (y = 0.10) micelles, respectively. The micelles are found to grow with respect to width (b) and, to a larger extent, length (c) with increasing c_t.

Table 1 Results from least-square model fitting analysis of SANS data. Dimensional properties (a, b, c, $\langle L\rangle$ and l_p) are given in units of Ångström (Å)

	$y = 0$	$y = 0.05$	$y = 0.10$	$y = 0.15$	$y = 0.20$	$y = 0.25$	$y = 0.30$
40 mM	Ellipsoids $a = 20.9$ $b = 28.2$ $c = 36.5$ $N = 151$ $\alpha = 0.19$ $c_{el} = 4$ mM $c_{mic} = 39$ mM	Ellipsoids $a = 20.8$ $b = 29.9$ $c = 38.9$ $N = 174$ $\alpha = 0.18$ $c_{el} = 5$ mM $c_{mic} = 38$ mM	Ellipsoids $a = 20.7$ $b = 31.5$ $c = 43.9$ $N = 212$ $\alpha = 0.17$ $c_{el} = 6$ mM $c_{mic} = 36$ mM	Polydisperse rods $a = 18.2$ $b = 29.1$ $\langle L\rangle = 130$ $N = 391$ $\sigma_L/\langle L\rangle = 0.61$ $\alpha = 0.11$ $c_{el} = 7$ mM $c_{mic} = 17$ mM	Polydisperse rods $a = 18.3$ $b = 27.8$ $\langle L\rangle = 600$ $N = 1790$ $\sigma_L/\langle L\rangle = 0.16$ $\alpha = 0.01$ $c_{el} = 1$ mM $c_{mic} = 67$ mM	Polydisperse rods $a = 18.4$ $b = 29.1$ $\langle L\rangle = 740$ $N = 3000$ $\sigma_L/\langle L\rangle = 0.18$ $\alpha = 0.01$ $c_{el} = 1$ mM $c_{mic} = 65$ mM	Polydisperse worms $a = 18.1$ $b = 32.3$ $l_p = 107$
20 mM	Ellipsoids $a = 20.8$ $b = 27.3$ $c = 34.7$ $N = 138$ $\alpha = 0.17$ $c_{el} = 2$ mM $c_{mic} = 19$ mM	Ellipsoids $a = 20.7$ $b = 28.7$ $c = 36.7$ $N = 157$ $\alpha = 0.17$ $c_{el} = 3$ mM $c_{mic} = 19$ mM	Ellipsoids $a = 20.7$ $b = 30.4$ $c = 40.0$ $N = 186$ $\alpha = 0.16$ $c_{el} = 3$ mM $c_{mic} = 19$ mM	Ellipsoids $a = 20.6$ $b = 32.0$ $c = 45.5$ $N = 228$ $\alpha = 0.15$ $c_{el} = 4$ mM $c_{mic} = 18$ mM	Polydisperse rods $a = 18.4$ $b = 31.2$ $\langle L\rangle = 95.7$ $N = 322$ $\sigma_L/\langle L\rangle = 0.77$ $\alpha = 0.16$ $c_{el} = 4$ mM $c_{mic} = 4.4$ mM	Polydisperse rods $a = 18.4$ $b = 28.7$ $\langle L\rangle = 560$ $N = 1780$ $\sigma_L/\langle L\rangle = 0.32$ $\alpha = 0.03$ $c_{el} = 2$ mM $c_{mic} = 18$ mM	Polydisperse rods $a = 18.3$ $b = 31.3$ $\langle L\rangle = 1110$ $N = 3900$ $\sigma_L/\langle L\rangle = 0.23$ $\alpha = 0.01$ $c_{el} = 6$ mM $c_{mic} = 24$ mM
10 mM	Ellipsoids $a = 20.4$ $b = 27.0$ $c = 32.5$ $N = 125$ $\alpha = 0.16$ $c_{el} = 1$ mM $c_{mic} = 9$ mM	Ellipsoids $a = 20.5$ $b = 27.8$ $c = 34.4$ $N = 142$ $\alpha = 0.16$ $c_{el} = 1$ mM $c_{mic} = 9$ mM	Ellipsoids $a = 20.5$ $b = 29.6$ $c = 36.6$ $N = 164$ $\alpha = 0.13$ $c_{el} = 1$ mM $c_{mic} = 9$ mM	Ellipsoids $a = 20.5$ $b = 31.3$ $c = 40.8$ $N = 199$ $\alpha = 0.21$ $c_{el} = 3$ mM $c_{mic} = 9$ mM	Ellipsoids $a = 20.3$ $b = 33.1$ $c = 45.9$ $N = 242$ $\alpha = 0.18$ $c_{el} = 3$ mM $c_{mic} = 8$ mM	Polydisperse rods $a = 18.5$ $b = 33.8$ $\langle L\rangle = 86.9$ $N = 330$ $\sigma_L/\langle L\rangle = 0.75$ $\alpha = 1.6$ $c_{el} = 11$ mM $c_{mic} = 2$ mM	Polydisperse rods $a = 18.2$ $b = 31.1$ $\langle L\rangle = 547$ $N = 1920$ $\sigma_L/\langle L\rangle = 0.22$ $\alpha = 0.10$ $c_{el} = 4$ mM $c_{mic} = 7$ mM

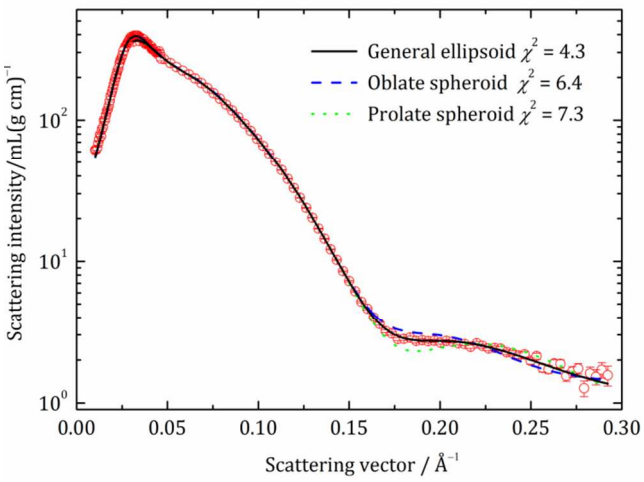

Fig. 1 Normalized scattering cross section as a function of the scattering vector q for CTAB in deuterium oxide at an overall surfactant concentration [CTAB] = 20 mM. Symbols represent SANS data and the lines represent the best available fit with a model for general ellipsoids (solid line), oblate spheroids (dashed line) and prolate spheroids (dotted line). The quality of the fits as measured by χ^2 is 4.3 (solid line), 6.4 (dashed line) and 7.3 (dotted line). The result of the best fit is given in Table 1.

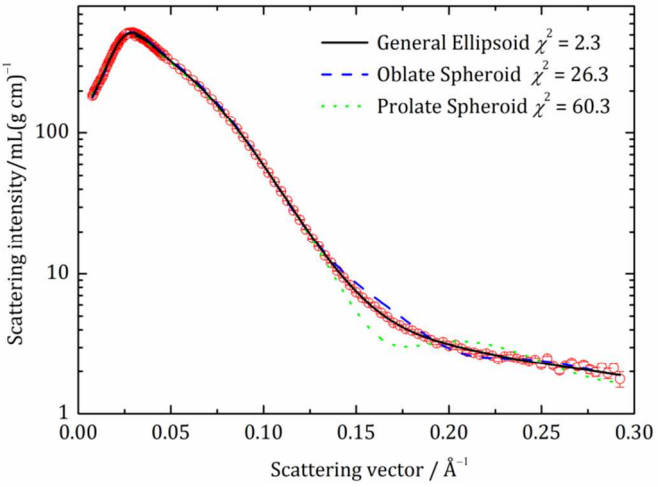

Fig. 2 Normalized scattering cross section as a function of the scattering vector q for a mixture of SOS and CTAB in deuterium oxide at a given mole fraction of SOS in solution $y = 0.15$ and an overall surfactant concentration [CTAB] + [SOS] = 20 mM. Symbols represent SANS data and the lines represent the best available fit with a model for general ellipsoids (solid line), oblate spheroids (dashed line) and prolate spheroids (dotted line). The quality of the fits as measured by χ^2 is 2.3 (solid line), 26.3 (dashed line) and 60.3 (dotted line). The result of the best fit is given in Table 1.

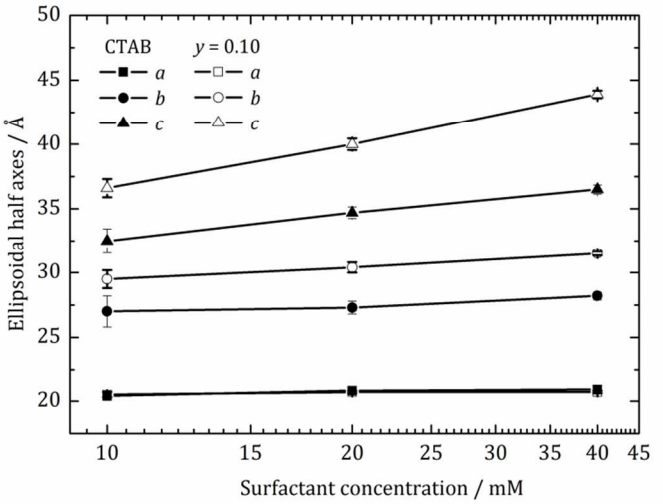

Fig. 3 Half axes related to thickness (squares), width (circles) and length (triangles), as determined by the SANS data analyses, plotted against the total concentration of surfactants [CTAB] + [SOS]. Filled symbols corresponds to pure CTAB micelles whereas open symbols represents mixed micelles with mole fraction of SOS y = 0.10.

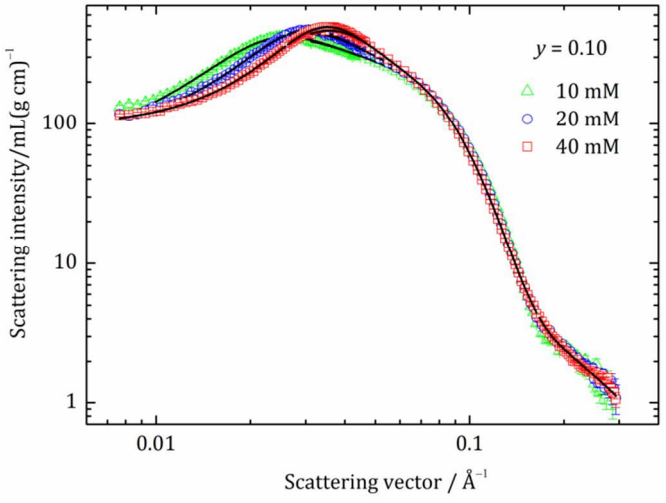

Fig. 4 Normalized scattering cross section as a function of the scattering vector q for mixtures of CTAB and SOS in deuterium oxide for a given mole fraction of SOS in solution y = 0.10. The overall surfactant concentrations of the samples are [SOS] + [CTAB] = 40 mM (squares), 20 mM (circles) and 10 mM (triangles). Symbols represent SANS data and the solid lines represent the best available fits with a model for general ellipsoids. The results of the fits are given in Table 1. The quality of the fits as measured by χ^2 is 3.5 (squares), 2.4 (circles) and 2.6 (triangles).

3.1.2 Growth behaviour of mixed CTAB/SOS micelles. Examples of normalized SANS data together with model fits for mixed micelles that grow moderately with surfactant concentration (y = 0.10) are shown in Fig. 4. Intermicellar interactions increase strongly with increasing concentration of micelles and has an obvious impact on the scattering data displayed as a decrease in the scattering intensity below about q = 0.03 Å^{-1}. Nevertheless, the micelles are found from our SANS data analysis to grow slightly in size with increasing surfactant concentration. Due to the interactions this growth in size is less obvious from the appearances of the scattering curves than for a system of more weakly interacting micelles. The consequences of the micellar growth may, nevertheless, be seen as a slight increase in scattering intensity in the vicinity of the maxima of the curves.

The aggregation numbers N have been calculated from the geometrical dimensions of the micelles by simply dividing the volume of a micelle with the average surfactant molecular volume. N is included in Table 1 as well as plotted against the surfactant concentration in Fig. 5. The aggregation number is found to monotonously increase with surfactant concentration c_t for a given composition y. The smallest micelles are formed in pure CTAB solutions and the aggregation number (N > 125) is found to considerably exceed the value (N_{max} = 95) consistent with strictly spherical micelles as calculated from the procedure suggested by Tanford[1,34]. For low fractions of SOS, *i.e.* $y \leq 0.10$, the aggregation number grow rather weakly with increasing surfactant concentration and the micelles are found to be shaped as fairly monodisperse ellipsoids at all investigated concentrations.

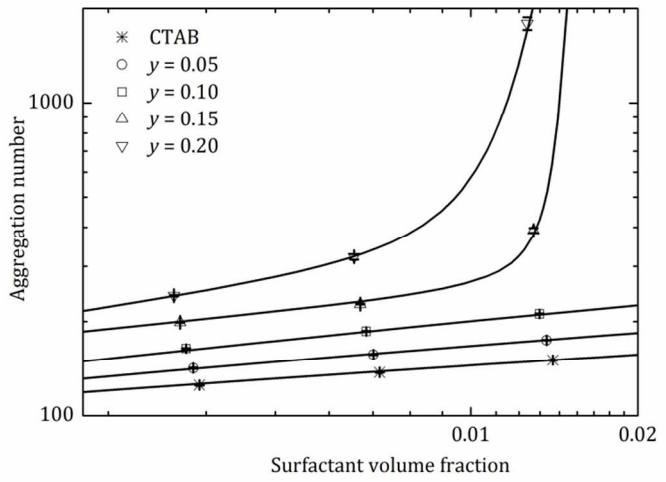

Fig. 5 The micelle aggregation number (N) plotted against volume fraction of surfactants aggregated in micelles at different mole fraction of SOS. Symbols represent experimental data obtained from SANS data analyses at different mole fractions of SDS (y = 0 (asterisk), y = 0.05 (circles), y = 0.10 (squares), y = 0.15 (up triangles) and y = 0.20 (down triangles). The lines represents theoretical predictions from the general micelle model, where the three bending elasticity constants H_0, k_c and $\overline{k}_c$ have been optimized to generate best agreement between theory and data. The resulting values of H_0, k_c and $\overline{k}_c$ are given in Table 2.

The corresponding N versus c_t plot may rather accurately be described with the linear function $N = A + B\ln(c_t/\text{mM})$ with values of intercept and slope equal to A = 81.8, B =

18.8 (y = 0), A = 88.5, B = 23.1 (y = 0.05) and A = 83.6, B = 34.6 (y = 0.10). The critical micelle concentration (cmc) for CTAB is about 1 mM which means that the intercept (A) roughly corresponds to the aggregation number at cmc. It is found to be rather constant for the three series and agrees well with the previously determined number N = 91 (in H_2O at 35 °C) obtained with static light scattering.[42] Notably, by means of extrapolating the experimentally determined half axes b and c for pure CTAB micelles one obtains almost oblate spheroidal micelles with a = 20 Å, b = 24.7 Å and c = 25.9 Å at cmc ≈ 1 mM. In contrast to the intercept, the slope (B) is found to increase significantly with y, indicating that the micelles grow increasingly stronger as the fraction of SOS in the micelles is increased.

SANS data for the composition y = 0.20, together with model fits, are shown in Fig. 6 for different total surfactant concentrations. It is evident from the increase in scattering intensity in the low-q regime that the aggregation number changes more conspicuously with surfactant composition at higher fractions of SOS. In accordance, when increasing c_t above 20 mM at y = 0.15 and 0.20, N raises dramatically and the quality of the model fits could be significantly improved by employing a model for polydisperse rods with volume-weighted average length $\langle L \rangle$ and an elliptical cross-section with half axis a and b, rather than a model for monodisperse ellipsoids. This sudden change in the extent of growth above a certain surfactant concentration has previously been observed for several systems and is often referred to as *the second cmc*.[2,4-7] It is generally believed that the appearance of a second cmc indicates the transition from spherical micelles, which grow only weakly with c_t, to rod-shaped micelles that are expected to show much stronger growth behaviour. However, the aggregation numbers of mixed CTAB/SOS micelles at the second cmc are found to be larger than about N = 200 or 300, *i.e.* far beyond aggregation numbers consistent with the presence of strictly spherical micelles with a maximum radius set by the length of a fully stretched out C_{16} tail, *i.e.* N_{max} = 101 at y = 0.15 and N_{max} = 103 at y = 0.20 (see ESI for calculations). Notably, a sudden growth of small spheroidal or ellipsoidal to much larger rodlike or wormlike micelles was also recently observed in SOS-rich samples of SOS and CTAB by changing the surfactant concentration slightly before the point of transition to bilayer aggregates.[20,21]

Further increasing the amount of SOS, the second cmc is shifted to even lower concentrations. In accordance, long polydisperse rodlike micelles are observed at all measured concentrations at y = 0.25, indicating that the second cmc is lower than 10 mM. The micelles grow strongly with increasing surfactant concentration. At y = 0.30 the micelles grow beyond 1000 Å and at 40 mM long wormlike or threadlike micelles are present that are too large for their size to be determined with SANS. At y = 0.35, long threadlike micelles are found to coexist with vesicles and other bilayer aggregates.

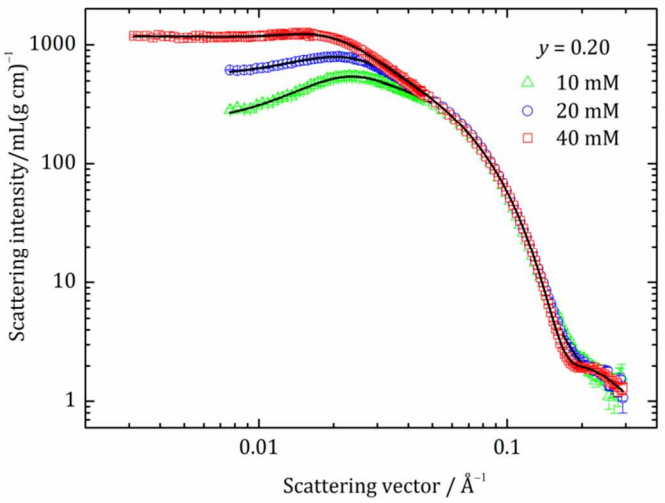

Fig. 6 Normalized scattering cross section as a function of the scattering vector q for mixtures of CTAB and SOS in deuterium oxide for a given mole fraction of SOS in solution y = 0.20. The overall surfactant concentrations of the samples are [SOS] + [CTAB] = 40 mM (squares), 20 mM (circles) and 10 mM (triangles). Symbols represent SANS data and the solid lines represent the best available fits with a model for general ellipsoids (triangles) or polydisperse rodlike micelles with an elliptical cross-section (squares and circles). The results of the fits are given in Table 1. The quality of the fits as measured by χ^2 is 3.7 (squares), 2.2 (circles) and 1.6 (triangles).

As discussed above, the structure factor we have employed in the SANS data analysis is strictly valid for rather small and compact micelles. Hence, the structure factor is expected to underestimate intermicellar interactions for substantially elongated and polydisperse micelles. As a result, the aggregation numbers as obtained for samples where data were fitted with a model for long and polydisperse micelles are probably somewhat underestimated. This effect is expected to increase with increasing size of the micelles. Hence, there are reasons to believe that the extent of micellar growth at y = 0.25 and 0.30, in reality, is considerably stronger than indicated from our fitting results displayed in Table 1.

3.1.3 Geometrical shape of mixed CTAB/SOS micelles. In Fig. 7 the half axis related to length (c) (or $\langle L \rangle$/2 for samples that were best fitted with the model for polydisperse rods) is plotted against c_t for the various compositions. It is seen that the dependence of the length of the micelles on surfactant concentration follows closely the corresponding behaviour of the aggregation number. In accordance, the micelle length is found to increase only slightly with c_t for pure CTAB micelles as well as mixed micelles with y = 0.05 and 0.10, whereas the length increases more abruptly above about c_t = 20 mM at y = 0.15 and 0.20 as the second cmc is reached.

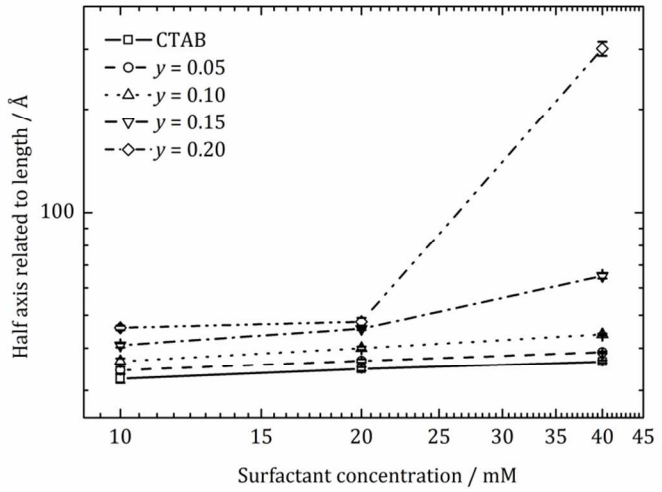

Fig. 7 The half axis related to length (*c*) of ellipsoidal micelles or the average half-length of polydisperse rods $\langle L\rangle/2$, as determined by the SANS data analyses, plotted against the total concentration of surfactants [CTAB] + [SOS] at different mole fraction of SOS, y = 0 (squares), y = 0.05 (circles), y = 0.10 (up triangles), y = 0.15 (down triangles) and y = 0.20 (diamonds).

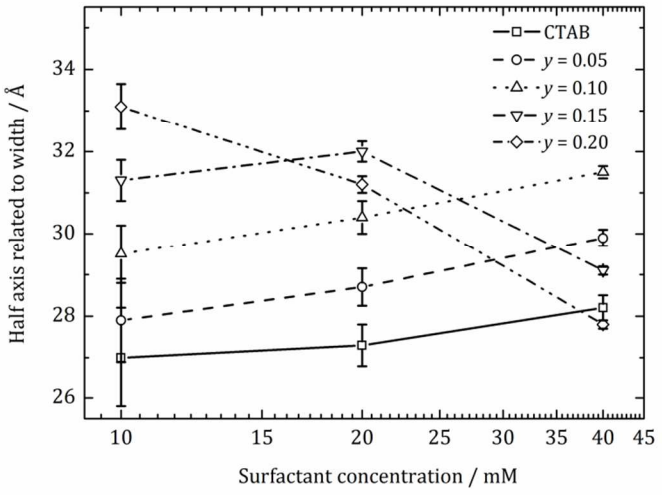

Fig. 8 The half axis related to width (*b*), as determined by the SANS data analyses, plotted against the total concentration of surfactants [CTAB] + [SOS] at different mole fraction of SOS, y = 0 (squares), y = 0.05 (circles), y = 0.10 (up triangles), y = 0.15 (down triangles) and y = 0.20 (diamonds).

Fig. 8 shows the corresponding plot for the half axis related to the width. The change in width also shows a strong correlation to the micellar growth behaviour. Most interestingly, it looks completely different as compared to the behaviours of aggregation number and length. In accordance, the micelle width is found to increase slightly with surfactant concentration for the three compositions where micelles grow weakly with c_t, *i.e.* y = 0, 0.05 and 0.10. At y = 0.15 the width also increases slightly in the weakly growing regime as c_t is increased from 10 to 20 mM. However, as c_t is increased beyond 20 mM, *i.e.* the concentration above which N and $\langle L\rangle$ increases dramatically with c_t as the second cmc is reached, the width is found to *decrease* with increasing c_t. This behaviour is even more evident for the composition y = 0.20, where the micelle width is found to monotonously decrease with increasing c_t in the entire regime of measured concentrations in-between 10 and 40 mM.

3.2 Theoretical calculations and comparison with experiments

3.2.1 The general micelle model. We have recently demonstrated that the behaviour of generally shaped triaxial micelles with distinct thickness, width and length may be rationalized from a theoretical point of view by the general micelle model.[22] The general micelle model combines thermodynamics of self-assembly with bending elasticity theory and may be described by the following relation that gives the volume fraction ϕ_{mic} of surfactants aggregated in triaxial, generally shaped, micelles as a function of the dimensionless half width r [22]

$$\phi_{mic} = \frac{\pi\xi^6 e^{-\alpha}}{\hat{v}^2}\int_0^\infty \frac{8r^2+6\pi r+\pi^2}{\beta+4\lambda r}\, e^{-\delta\psi(r)-\pi\beta r-2\pi\lambda r^2}dr \quad (3)$$

The theory is based on the geometrical model of triaxial tablet-shaped shown in Fig. S1 in the ESI. The general micelle model demonstrates that at least three parameters are necessary to fully describe the behaviour of surfactant micelles. In accordance with the Helfrich expression[43], the three bending elasticity constants spontaneous curvature (H_0), bending rigidity (k_c) and saddle splay constant ($\bar{k}_c$) are able to describe different aspects of a curved surfactant monolayer, for instance a micelle. The three bending elasticity constants may be interpreted as thermodynamic parameters and calculated from a suitable molecular model by means of minimizing the free energy per molecule of a surfactant interfacial layer at given values of H and K.[44-46]

The additional quantities that appear in eqn (3) are defined as follows. ξ denotes the half thickness of the tablet-shaped micelles and $\hat{v}$ is the average surfactant volume. $\lambda \equiv \xi^2\gamma_p/kT$ is the reduced and γ_p the real planar interfacial tension of a self-assembled interface. $\alpha \equiv 2\pi\left(3k_c + 2\bar{k}_c - 8\xi k_c H_0\right)/kT + 4\pi\lambda$, $\beta \equiv \pi k_c(1 - 4\xi H_0)/kT + 2\pi\lambda$ and $\delta \equiv 2\pi k_c/kT$ are three dimensionless parameters taking into account the bending free energy. The ψ-function ($0 < \psi < 1$) equals unity in the limit $r \to 0$ and zero as $r \to \infty$. More details, including the derivation of eqn (3), are provided in ref 22.

The distributions in length and width of generally shaped micelles may be deduced from eqn (3) and, as a result, it is straight forward to calculate the average width $\langle\Omega\rangle \equiv 2(\langle R\rangle + \xi)$ and length $\langle\Lambda\rangle \equiv \langle L\rangle + \langle\Omega\rangle$ as functions of the concentrations of aggregated surfactants. By means of dividing the average volume of a micelle with the average surfactant molecular volume it is thus straight forward to calculate the micelle aggregation number as a function of ϕ_{mic} and surfactant concentration.

3.2.2 Growth behaviour and aggregation number. In accordance with our experimental results, we have set the half thickness of the micelles equal to $\xi = 20$ Å in eqn (3) for all surfactant compositions whereas the molecular volume was set to its appropriate value $\hat{v} = x\hat{v}_{SOS} + (1-x)\hat{v}_{CTAB}$. This leaves the three bending elasticity constants H_0, k_c and $\overline{k}_c$ as unknown parameters in eqn (3). Hence, by means of optimizing the agreement between theory and experimental aggregation numbers with respect to H_0, k_c and $\overline{k}_c$ we are able to generate theoretical growth curves. Thus, the aggregation numbers of mixed CTAB/SOS micelles, as predicted from the general micelle model, as functions of the volume fraction of aggregated surfactant are plotted in Fig. 5, together with experimental results, for the different compositions we have investigated and the resulting values of H_0, k_c and $\overline{k}_c$ are tabulated in Table 2.

Table 2 The bending elasticity constants bending rigidity (k_c), saddle-splay constant ($\overline{k}_c$) and half micellar thickness times spontaneous curvature (ξH_0) as obtained by optimizing the agreement between the general micelle model and experimental results

	k_c/kT	$\overline{k}_c/kT$	ξH_0	$\xi k_c H_0/kT$
CTAB	3.4	< -11.5	> 0.45	> 1.5
$y = 0.05$	3.0	< -8.0	> 0.37	> 1.1
$y = 0.10$	2.6	< -4.0	> 0.31	> 0.81
$y = 0.15$	2.3	1.35	0.38	0.87
$y = 0.20$	1.5	9.1	0.36	0.54

The general micelle model predicts weakly growing micelles at low surfactant concentrations followed by a rather sharp and progressively steeper increase in N above concentrations roughly corresponding to the second cmc, in very good agreement with experiments. Since the three bending elasticity constants H_0, k_c and $\overline{k}_c$ influence the growth curves in fundamentally different ways, it is, in principle, possible to unambiguously determine all three bending elasticity constants from experimental growth curves comprising at least three aggregation numbers below as well as above the second cmc. The statistical errors of the aggregation numbers shown in Fig. 5 are very small and the detailed appearance of the growth curves is very sensitive to each of the three bending constants. As a result, the three parameters are virtually uncorrelated and can be determined rather accurately from our data. This is supported by the reasonable values and trends of the resulting H_0, k_c and $\overline{k}_c$ as given in Table 2.

The saddle-splay constant is expected to influence the size of a self-assembled surfactant aggregate, thus favouring large aggregates for high values of $\overline{k}_c$.[47,48] For micelles, it turns out that the saddle-splay constant mainly has the effect of shifting the curve along the x-axis, which means that its value is largely determined by the location of the second cmc at the sharp increase in aggregation number. The higher value of $\overline{k}_c$, the lower is the second cmc. At low fractions of SOS, *i.e.* y = 0, 0.05 and 0.10, a second cmc is never observed in the range of measured concentrations. This simply means that $\overline{k}_c$ is too low for the second cmc to appear in our experimental results and we may only conclude that $\overline{k}_c$ must fall below a certain value as indicated in Table 2. Sufficiently low values of $\overline{k}_c$ may correspond to a second cmc close to, or even above, $\phi_{mic} = 1$ implying that the micelles will grow moderately in the entire range of surfactant concentrations.

The spontaneous curvature is expected to directly influence the size of micelles since the micelles become less curved as the aggregation number increases.[48] It is found that H_0 mainly has the effect of shifting the curve vertically along the y-axis, while influencing the second cmc only slightly. Thus, lower values of H_0 correspond to higher values of N and vice versa. In the cases where a second cmc is not observed within the range of measured surfactant concentrations (y = 0, 0.05 and 0.10), and we are not able to determine $\overline{k}_c$, H_0 as determined from the optimization depends on the chosen value of $\overline{k}_c$ which means that we are only able to determine a minimum value of H_0 as indicated in Table 2. Notably, we have chosen to include $k_c H_0$, in addition to H_0, in Table 2 since this quantity is easier to physically interpret than the bare spontaneous curvature H_0.[44,45,49]

The always positive quantity bending rigidity k_c has no direct influence on the size of surfactant aggregates but is related to the geometrical heterogeneity of the aggregates.[22,48] In accordance, low values of k_c promote a high polydispersity of the aggregates.[31] For micelles it follows that k_c determines the appearance of the N versus ϕ_{mic} curve in the way that high values of k_c gives a rather sharp and abrupt increase of N at the second cmc, whereas the growth behaviour appears smoother and the second cmc less well-defined as k_c assumes lower values. This difference in appearance of the growth curves is clearly seen for the two cases $y = 0.15$ ($k_c/kT = 2.3$) and $y = 0.20$ ($k_c/kT = 1.5$) in Fig. 5.

It is also possible to determine k_c from the growth curves at y = 0, 0.05 and 0.10 that are located below the second cmc, assuming that the experimental values are still fairly close to the second cmc. Here, k_c determines the slope of the nearly linear curves shown in Fig. 5. Thus, the slope increases in magnitude with decreasing values of k_c. As a result, the bending rigidity is found to decrease with increasing mole fraction of SOS, *i.e.* $k_c/kT = 3.4$ ($y = 0$), 3.0 ($y = 0.05$) and 2.6 ($y = 0.10$), for mixed CTAB/SOS micelles.

This decrease in bending rigidity with increasing fraction of SOS is in qualitative agreement with theoretical estimates according to which the process of mixing surfactants have an explicit effect to reduce the magnitude of k_c.[50-52] This effect is expected to be particularly evident in mixtures of two oppositely charged surfactants.[45] Notably, the derivative of N with respect to surfactant concentration is directly related to the polydispersity through eqn (1), which means that k_c is expected to directly influence the polydispersity of micelles (see section 3.3 below).

3.2.3 The geometrical shape and its correlation with growth behaviour. The general micelle model not only predicts the change in aggregation numbers with surfactant concentration as shown in Fig. 5. The theory also predicts the geometrical shape of micelles and its relation to the growth behaviours. In Figs. 9 and 10 we have plotted the average length ⟨Λ⟩ and width ⟨Ω⟩, respectively, of micelles, as theoretically predicted by the general micelle model, against volume fraction of surfactant aggregated in micelles. The length is found to depend on surfactant concentration in a similar way as the aggregation number does according to Fig. 5. As a result, the curves much resemble the experimental plots of the half axis related to length (*c*) versus surfactant concentration shown in Fig. 7.

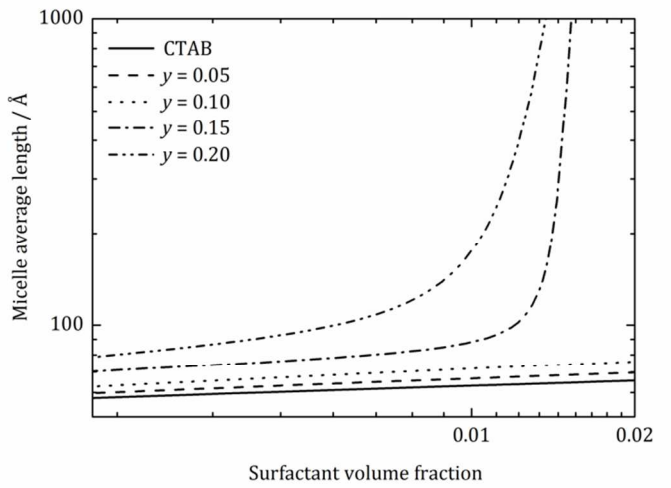

Fig. 9 The average length (⟨Λ⟩) of micelles plotted against volume fraction of surfactants aggregated in micelles at different mole fraction of SOS. The lines represent theoretical predictions using the general micelle model with the bending elasticity constants H_0, k_c and $\overline{k}_c$ set to their optimized values given in Table 2.

Most interestingly, the theoretically obtained micelle widths plotted in Fig. 10 behave in the same way as the experimentally obtained half axis related to width (*b*) shown in Fig. 8. In accordance with both theory and experiments, the micelle width is found to slightly increase with concentration in regions where micelles grow weakly, whereas the width reaches a maximum *and begins to decrease* in regimes above the second cmc where micelles grow strongly.

Hence, we are able to conclude that, according to both experiments and theoretical predictions, there is a strong correlation between growth behaviour and geometrical shape of the micelles. The weak growth behaviour found at $y = 0$, 0.05 and 0.10, and at low concentrations at $y = 0.15$ and 0.20, may be rationalized as a consequence of the fact that the local curvature of the micelle interfaces changes with increasing aggregation number as both width and length increases in magnitude. In accordance, the extent of the micellar growth is inhibited in this region by an energetic penalty due to changes in local curvature.

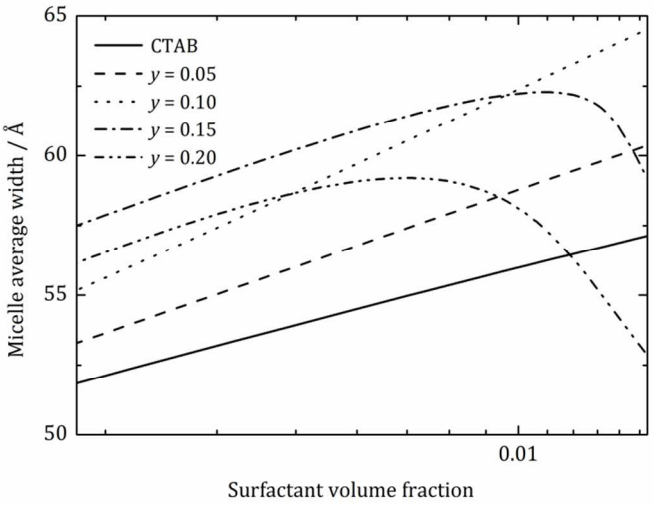

Fig. 10 The average width (⟨Ω⟩) of micelles plotted against volume fraction of surfactants aggregated in micelles at different mole fraction of SOS. The lines represent theoretical predictions using the general micelle model with the bending elasticity constants H_0, k_c and $\overline{k}_c$ set to their optimized values given in Table 2.

According to both theory and experiments at $y = 0.15$, micelles grow more strongly in length, whereas the width is found to decrease, above about the second cmc. The maximum in width is found at about $\phi_{mic} = 0.02$ in the theoretical curve for $y = 0.15$ [*cf.* Fig. 10], which roughly corresponds to $c_{mic} = 60$ mM. In contrast, the maximum in width is located at about 20 mM according to experiments [*cf.* Fig. 8]. Likewise, according to the experimental results for $y = 0.20$, shown in Fig. 8, *b* decreases in the entire range of measured concentrations, indicating that the maximum in width is located below $c_t = 10$ mM. The corresponding theoretical predictions imply a slight increase in width between $\phi_{mic} = 0.003$ and 0.006 (roughly corresponding to $c_t = 10$ and 20 mM, respectively) with a maximum located at $\phi_{mic} = 0.007$ (*i.e.* slightly above $c_t = 20$ mM). Despite this discrepancy between theory and experiments regarding the absolute location of the maximum in width, it is clearly seen, as the two theoretical curves for compositions $y = 0.15$ and 0.20 in Fig. 10 are compared, that the maximum in width is significantly shifted towards lower surfactant concentrations as the fraction of SOS is raised, in agreement with the experimental observations displayed in Fig. 8.

The experimental observations of the second cmc, as well as of the width of micelles reaching a maximum followed by a decrease as the surfactant concentration is raised beyond the second cmc, may be rationalized as a result of micellar curvature effects taken into account by the general micelle model. The driving force for micelles to grow in width, in addition to length, is the reduction in curvature energy of the semi-toroidal end caps. We have previously

demonstrated that, in accordance with the general micelle model, the width and length within a size distribution of triaxial tablet-shaped micelles, are coupled in the free energy expression for tablet-shaped micelles.[22,53] As a consequence, width and length are strongly correlated. Thus, the width always decreases with increasing length within a single distribution of micelles with different lengths and widths. This means that micelles, in order to grow substantially in length, must reduce their width. As a consequence, micelles become less wide, and more resembles spherocylindrical micelles, as they grow sufficiently long. However, decreasing the width means that the curvature energy is raised and, in order to counteract this increase in end cap curvature energy, the micelles start to grow more strongly in length, thus reducing the number of micelles and unfavourable end caps.

3.3 Polydispersity of mixed CTAB/SOS micelles.

It is possible to calculate the polydispersity as a function of surfactant concentration for any given function of N versus ϕ_{mic} using the important relation derived by Hall and Pethica[11] shown in eqn (1). As a result, it is possible to determine the polydispersity of micellar systems once the growth behaviour is understood from a theoretical point of view. In accordance, we have plotted the volume-weighted relative standard deviation $\sigma_N/\langle N\rangle$ as a function of ϕ_{mic} in Fig. 11 for the various investigated surfactant compositions of mixed CTAB/SOS micelles. It is seen that the polydispersity, as expected, is rather low for weakly growing micelles and increases slightly from about $\sigma_N/\langle N\rangle = 0.35$ ($y = 0$) to 0.45 ($y = 0.10$) depending on surfactant composition. The polydispersity is found to be fairly constant with respect to surfactant concentration (as a matter of fact it slightly decreases with ϕ_{mic}). At the compositions $y = 0.15$ and 0.20, $\sigma_N/\langle N\rangle$ is fairly constant, equalling about 0.5, at low surfactant concentrations, but increases sharply above the second cmc and may eventually exceed unity.

The trends in polydispersity shown in Fig. 11 qualitatively agree very well with our experimental observations. In accordance, the SANS data for weakly growing micelles formed at low fractions of SOS, as well as at low surfactant concentration at higher fractions of SOS $y = 0.15$ and 0.20, could be fitted with a model for monodisperse ellipsoidal micelles. On the other hand, it was necessary to include polydispersity in the models used to fit data for samples above the second cmc. However, the quantitative numbers for $\sigma_L/\langle L\rangle$, as obtained from our SANS data analysis for polydisperse rodlike micelles and included in Table 1, appears considerably smaller than expected from the observed growth behaviour. Probably, comparatively strong intermicellar interactions among substantially elongated micelles may interfere and influence the scattering data so that the apparent polydispersity becomes underestimated and significantly lower as compared to reality. Nevertheless, the polydispersity $\sigma_L/\langle L\rangle = 0.77$, as obtained from our model fitting analysis for the sample [$y = 0.20$, 20 mM] (corresponding to $\phi_{mic} \approx 0.006$), is in fair agreement with the result shown in Fig. 11.

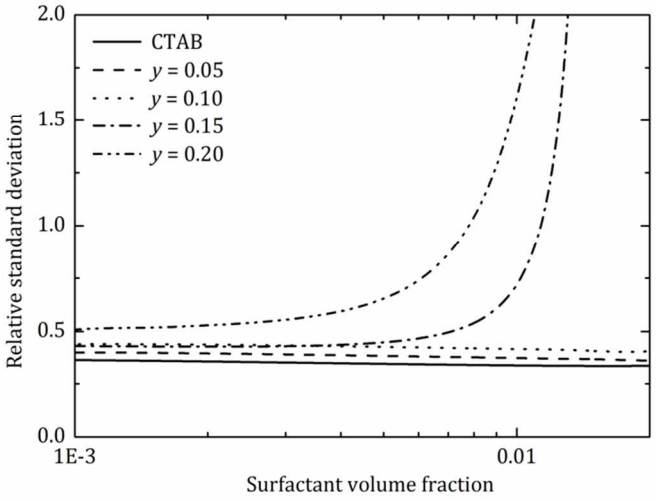

Fig. 11 The relative standard deviation $\sigma_N/\langle N\rangle$ of mixed CTAB/SOS micelles at different mole fractions of SDS ($y = 0$ (solid line), $y = 0.05$ (dashed line), $y = 0.10$ (dotted line), $y = 0.15$ (dash-dotted line) and $y = 0.20$ (dash-dot-dotted line). The lines have been as calculated using eqn (1) for the various theoretical curves shown in Fig. 5.

A polydispersity equal to $\sigma_N/\langle N\rangle = 1$, as expected for strictly spherocylindrical micelles in the limit of large aggregation numbers[48,54,55], corresponds to $d\ln N/d\ln \phi_{mic} = N$ in accordance with eqn (1). As a result, the spherocylindrical micelle model appears to underestimate the polydispersity as well as the extent of growth of micelles formed above the second cmc. As a matter of fact, enormous concentration-induced growth behaviours, exceeding $d\ln N/d\ln \phi_{mic} = 1$, have frequently been observed in systems with long wormlike micelles.[14-16]

Conclusions

We have demonstrated, using small angle-neutron scattering, that the growth behaviour of mixed CTAB-rich hexadecyl trimethylammonium bromide (CTAB)/sodium dodecyl sulphate (SOS) micelles is strongly influenced by the surfactant composition in the micelles. In accordance, pure CTAB micelles grow only weakly with increasing surfactant concentration, and the extent of growth increases slightly as a small amount of SOS is added. At higher SOS mole fractions, the micelle aggregation number is found to increase progressively from a weakly growing regime at low surfactant concentrations to a strongly growing regime above a certain concentration. This transition from a weakly to a strongly growing regime has frequently been observed in the past and is usually referred to as *the second cmc*.[2,4-7] Above this concentration, the extent of micellar growth becomes conspicuously strong. Moreover, from SANS data

analysis we have been able to determine the detailed geometrical shape of the micelles in order to correlate changes in geometry with micellar growth behaviour. It turns out that micelles grow weakly with respect to both width and length at low SOS mole fractions, as well at low surfactant concentrations at higher fractions of SOS, whereas the length increases strongly while the width decreases above the second cmc.

Our experimental results have been rationalized and compared with predictions deduced from the recently developed general micelle model[22]. The theory takes into account bending elasticity properties in terms of the three quantities spontaneous curvature (H_0), bending rigidity (k_c) and saddle-splay constant ($\overline{k}_c$). The theoretically predicted growth curves, as optimized with respects to H_0 k_c and $\overline{k}_c$, gives excellent agreement with experimental results. Moreover, the theoretical model predicts the observed change in micelle geometry with increasing surfactant concentration. That is, weakly growing micelles grow with respect both width and length whereas strongly growing micelles grow considerable in length while decreasing in width as the surfactant concentration is raised above the second cmc. In accordance with theoretical predictions, the growth behaviour may be rationalized as a consequence of changes in local curvature in the semi-toroidal end caps upon varying both width and length. This gives rise to a curvature energetic penalty, upon increasing both width and length, which inhibits the extent of growth of the micelles. As the micelles grow longer they become less wide due to a coupling between width and length in a micelle distribution. Consequently, the end cap curvature energy is raised for considerably elongated micelles and, as a result, the micelles start to grow more strongly in size in order to reduce the number of micelles and unfavourable end caps.

By means of optimizing the agreement between the general micelle model and experimental results we have been able to determine the three bending elasticity constants spontaneous curvature (H_0), bending rigidity (k_c) and saddle-splay constant ($\overline{k}_c$) for mixed CTAB/SOS micelles. It is found that both k_c and k_cH_0 decreases with an increasing mole fraction of SOS whereas $\overline{k}_c$ increases from negative values for pure CTAB micelles to positive values for mixed CTAB/SOS micelles that display a second cmc. These trends for all bending elasticity constants qualitatively agree with calculations using the Poisson-Boltzmann mean field theory for ionic surfactant systems.[41,45]

Acknowledgements

Institut Laue Langevin (ILL) is acknowledged for allocated SANS beam time (Proposal 9-10-1255).

Notes and references

[a] KTH Royal Institute of Technology, School of Chemical Science and Engineering,, Department of Chemistry, Surface and Corrosion Science, SE-10044 Stockholm, Sweden. E-mail: magnusbe@kth.se; Fax: +46 8 20 82 84, Tel: +46 8 790 99 21

[b] Institut Laue Langevin, DS/LSS, 6 rue Jules Horowitz, B.P. 156, 38042 Grenoble Cedex 9, France.

Electronic Supplementary Information (ESI) available: See
DOI: 10.1039/b000000x/

1 C. Tanford, *J. Phys. Chem.*, 1972, **76**, 3020-3024.
2 G. Porte, Y. Poggi, J. Appell and G. Maret, *J. Phys. Chem.*, 1984, **88**, 5713-5720.
3 P. Lianos, J. Lang and R. Zana, *J. Colloid Interface Sci.*, 1983, **91**, 276-279.
4 M. Törnblom, U. Henriksson and M. Ginley, *J. Phys. Chem.*, 1994, **98**, 7041-7051.
5 M. Törnblom, R. Stinikov and U. Henriksson, *J. Phys. Chem. B*, 2000, **104**, 1529-1538.
6 S. May and A. Ben-Shaul, *J. Phys. Chem. B*, 2001, **105**, 630-640.
7 A. González-Pérez, L. M. Varela, M. Garcia and J. R. Rodriguez, *J. Colloid Interface Sci.*, 2006, 293, 213-221.
8 B. Cabane, R. Duplessiz and T. Zemb, *J. Phys. France*, 1985, **46**, 2161-2179.
9 M. Bergström and J. S. Pedersen, *Phys. Chem. Chem. Phys*, 1999, **1**, 4437-4446.
10 L. M. Bergström and V. M. Garamus, *J. Colloid Interface Sci.*, 2012, **381**, 89-99.
11 D. G. Hall and B. A. Pethica, in *Nonionic Surfactants*, ed. M. J. Schick, Marcel Dekker, New York, 1967, vol. 1, pp. 516-557.
12 Y. Croonen, E. Geladé, M. Van der Zegel, M. Van der Auweraer, H. Vandendriessche, F. C. De Schryver and M. Almgren, *J. Phys. Chem.*, 1983, 87, 1426-1431.
13 F. H. Quina, P. M. Nassar, J. B. S. Bonilha and B. L. Bales, *J. Phys. Chem.*, 1995, **99**, 17028-17031.
14 P. Schurtenberger and C. Cavaco, *J. Phys II France*, 1993, **3**, 1279-1288.
15 P. Schurtenberger and C. Cavaco, *J. Phys II France*, 1994, **4**, 305-317.
16 P. Schurtenberger and C. Cavaco, *Langmuir*, 1996, 12, 2894-2899.
17 H. Pilsl, H. Hoffmann, S. Hoffmann, J. Kalus, A. W. Kencono, P. Lindner and W. Ulbricht, *J. Phys. Chem.*, 1993, **97**, 2745-2754.
18 M. Bergström and J. S. Pedersen, *Langmuir*, 1999, **15**, 2250-2253.
19 S. Prévost, L. Wattebled, A. Laschewsky and M. Gradzielski, *Langmuir*, 2011, **27**, 582-591.
20 L. M. Bergström, S. Skoglund, K. Edwards, J. Eriksson and I. Grillo, *Langmuir*, 2013, **29**, 11834-11848.
21 L. M. Bergström, S. Skoglund, J. Eriksson, K. Edwards and I. Grillo, *Langmuir*, 2014, **30**, 3928-3938.
22 L. M. Bergström, *ChemPhysChem*, 2007, **8**, 462-472.

23 J. P. Cotton, in *Neutron, X-Ray and Light Scattering: Introduction to an Investigative Tool for Colloidal and Polymeric Systems*, eds. P. Lindner and T. Zemb, North-Hollland, Amsterdam, 1991, pp. 3-18.
24 J. P. Cotton, in *Neutron, X-Ray and Light Scattering: Introduction to an Investigative Tool For Colloidal and Polymeric Systems*, eds. P. Lindner and T. Zemb, North-Holland, Amsterdam, 1991, pp. 19-31.
25 J. S. Pedersen, *Adv. Colloid Interface Sci.*, 1997, **70**, 171-210.
26 J. P. Hansen and J. B. Hayter, *Molec. Phys.*, 1982, **46**, 651-656.
27 J. B. Hayter and J. Penfold, *Molec. Phys.*, 1981, **42**, 109-118.
28 M. Kotlarchyk and S. H. Chen, *J. Chem. Phys.*, 1983, **79**, 2461-2469.
29 J. B. Hayter and J. Penfold, *Colloid and Polymer Science*, 1983, **261**, 1027-1030.
30 M. Bergström and J. S. Pedersen, *J. Phys. Chem. B*, 1999, **103**, 8502-8513.
31 L. M. Bergström, S. Skoglund, K. Danerlöv, V. M. Garamus and J. S. Pedersen, *Soft Matter*, 2011, **7**, 10935-10944.
32 L. M. Bergström and V. M. Garamus, *Langmuir*, 2012, **28**, 9311-9321.
33 C. Tanford, *The hydrophobic effect*, Wiley, New York, 1980.
34 Y. Chevalier and T. Zemb, *Rep. Prog. Phys.* , 1990, **53**, 279-371.
35 J. M. Corkill, J. M. Goodman and T. Walker, *Trans. Faraday Soc.*, 1967, **63**, 768-772.
36 L. M. Bergström and T. Bramer, *J. Colloid Interface Sci.*, 2008, **322**, 589-595.
37 L. M. Bergström and M. Aratono, *Soft Matter*, 2011, **7**, 8870 - 8879.
38 J. S. Pedersen, *J. Phys. IV (Paris) Coll. C8* 1993, **3**, 491-498.
39 J. S. Pedersen, D. Posselt and K. Mortensen, *J. Appl. Crystallogr.*, 1990, **23**, 321-333.
40 B. R. Bevington, *Data Reduction and Error Analysis for Physical Sciences*, McGraw-Hill, New York, 1969.
41 D. J. Mitchell and B. W. Ninham, *Langmuir*, 1989, **5**, 1121-1123.
42 T. Imae, R. Kamiya and S. Ikeda, *J. Colloid Interface Sci.*, 1985, **108**, 215-225.
43 W. Helfrich, *Z. Naturforsch. C*, 1973, **28**, 693-703.
44 L. M. Bergström, *Langmuir*, 2006, **22**, 3678-3691.
45 L. M. Bergström, *Langmuir*, 2006, **22**, 6796-6813.
46 L. M. Bergström, *Colloids Surf. A*, 2008, **316**, 15-26.
47 S. A. Safran, *Phys. Rev. A*, 1991, **43**, 2903-2904.
48 L. M. Bergström, in *Application of Thermodynamics to Biological and Material Science*, ed. M. Tadashi, InTech, Rijeka, 2011, vol. ch. 11, pp. 289-314.
49 L. M. Bergström, *Langmuir*, 2009, **25**, 1949-1960.
50 S. A. Safran, *Adv. Phys.*, 1999, **48**, 395-448.
51 M. M. Kozlov and W. Helfrich, *Langmuir*, 1992, **8**, 2792-2797.
52 G. Porte and C. Ligoure, *J. Chem. Phys.*, 1995, **102**, 4290-4298.
53 M. Bergström, *J. Chem. Phys.*, 2000, **113**, 5559-5568.
54 J. C. Eriksson and S. Ljunggren, *J. Chem. Soc., Faraday Trans. 2*, 1985, **81**, 1209-1242.
55 L. M. Bergström, *J. Colloid Interface Sci.*, 2006, **293**, 181-193.

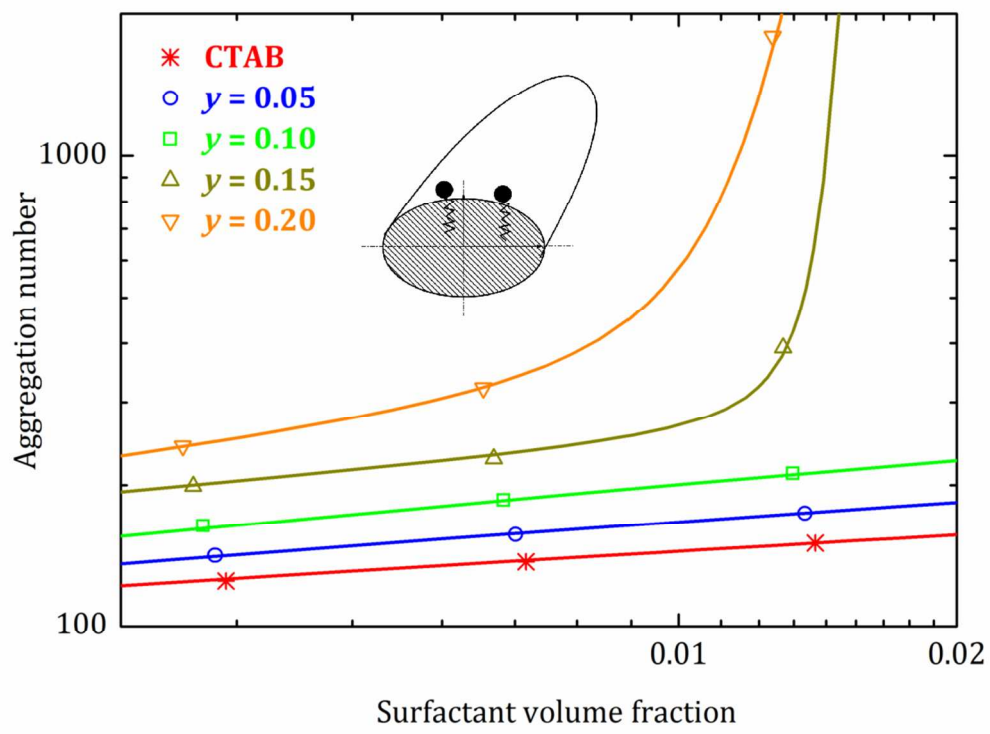

Growth behaviour and how it is related to geoemtrical shape of mixed CTAB/SOS micelles has been investigated with SANS
254x190mm (124 x 124 DPI)